Journal of Structural Geology, Vol. 11, No. 7, pp. 895 to 905, 1989
Printed in Great Britain

0191-8141/89 $03.00+0.00

Slickenside formation by surface melting during the mechanical excavation of rock

JOHN G. SPRAY

Department of Geology, University of New Brunswick, Fredericton, Canada E3B 5A3

(*Received* 6 *January* 1988; *accepted in revised form* 10 *May* 1989)

Abstract—This work discusses the nature and origin of slickensides generated by the impingement of high-carbon steel teeth on sandstone during the mechanical excavation of boulders by back shovel and front loader. The slickensides show a number of morphological features that can be related to the direction and sense of tooth displacement, including striations, carrot-shaped grooves, curved fractures and steps.

Scanning and transmission electron microscopy reveal that the slickensides comprise a layer of Fe-enriched, glass-bonded gouge (≤ 150 μm thick). The estimated shear stresses and velocities realized at the tooth–rock interface (175 MPa at 1 m s^{-1} for the back shovel and 100 MPa at 2 m s^{-1} for the front loader) indicate that a heat production of 150–200 MW m^{-2} and mean surface temperature of 1400–1700°C were achieved. XRF and microprobe analyses confirm that localized bulk melting and Fe-enrichment of the surface occurred during slip.

The excavator-generated slickensides provide an analogue for the effects of a single co-seismic event in the evolution of a shallow, relatively dry fault surface. From a simple consideration of energetics under these conditions, it is apparent that localized surface melting should be commonplace. Such an analogue may be useful as a guide for recognizing melt features in natural slickensides, features that would otherwise tend to be obscured during lengthier periods of interseismic surface modification.

INTRODUCTION

SLICKENSIDES are non-penetrative smoothed or polished surfaces normally developed on planes of movement, as found in fault zones and between rock layers folded by flexural slip (e.g. Tjia 1964, 1967, Hills 1972, Hobbs *et al.* 1976, Williams & Spray 1979). Many slickensides are also lineated with continuous or discontinuous grooves or ridges and may exhibit various other damage and accretionary features.

In addition to being potentially employed as displacement and sense of movement indicators in the field (e.g. Petit 1987), slickensides and related features have been used to infer the history of surface interaction, particularly as they may pertain to the earthquake cycle (e.g. Jaeger 1959, Brace & Byerlee 1966, Engelder 1974, Power & Tullis 1989). In this respect it has become evident that slickensides may undergo numerous cycles of modification via various co-seismic and interseismic events. Field and experimental evidence suggest that these modifications include melting (Friedman *et al.* 1974), gouge generation (Engelder 1974) and crystal growth (Durney & Ramsay 1973), although evidence of melting has not yet been unequivocally found in natural slickensides.

This work considers an analogue for a phase of slickenside development that involves surface melting. The experimental conditions replicate shear stresses, displacements and velocities of slip typical of seismogenic faulting. Heat production is comparable to that achieved for large earthquakes, although there is an obvious scaling difference.

Under conditions of relatively dry faulting it is likely that naturally occurring slickensides originate by surface melting during co-seismic slip. In the majority of cases, however, any evidence of melting will be obscured by subsequent interseismic devitrification and by the precipitation of new mineral phases on the modified surface. The simple co-seismic analogue described here may therefore help to distinguish a transient melting event from other episodes of slickenside development.

ROCK TYPE AND EXCAVATING CONDITIONS

The artificial slickensides were formed during back shovel and front loader excavation of rock during construction work in the Southwood Park area of Fredericton, New Brunswick. The predominant lithology in the region is a coarse-grained Pennsylvanian sandstone of fluvial origin (Barss & Hacquebard 1967). The sandstone does not occur *in situ* at the site of excavation but rather as small ($\approx 5 \times 10^{-4}$ m^3) to large (≈ 6 m^3) boulders embedded in a clayey soil. The sandstone consists of sub-angular grains of quartz, albite and alkali feldspar with lesser amounts of muscovite, epidote, magnetite, ilmenite, zircon and sphene, which together suggest derivation from a granitoid. These minerals are cemented by a matrix of quartz, clay minerals, chlorite, carbonate and barytes. Survival of the less resistant mineral phases and the preservation of relatively fresh albite within the sedimentary rock indicate that the sandstone is immature.

The slickenside structures were generated in two

situations: during extraction and manoeuvring of the larger boulders by crawler back shovel (model Link-Belt LS-3400 with Esco heavy duty bucket; operating weight 24,000 kg) and during sub-horizontal scraping of smaller boulders by wheeled front loader (model Caterpillar G936 with Caterpillar standard excavating bucket; operating weight 12,000 kg). Observation of the excavating operations established the velocities of bucket movement (back shovel ≈ 1 m s^{-1}; front loader ≈ 2 m s^{-1}) and approximate forces acting on the rock (e.g. when the front loader rode on its rear wheels and bucket, with front wheels elevated, approximately half its operating weight rested on the bucket).

Failure to grip the rock by the excavators resulted in surface scraping accompanied by a loud intermittent tearing sound (like rubbing a dry finger over a balloon) and an explosive release of rock powder and fragments from the rock surface (spalling).

Numerous runs were observed using this equipment and the velocity, load, duration and sense of tooth–rock interaction noted. Twelve samples of slickensides were then collected for analysis.

PREPARATORY AND ANALYTICAL TECHNIQUES

Slickenside fragments for topographic analysis using the scanning electron microscope (SEM) were gold-coated but otherwise unprepared (i.e. no epoxy was used). Samples for conventional petrographic microscopy, microprobe analysis and TEM were protected with a coating of epoxy resin and vacuum impregnated with a low-viscosity epoxy prior to sawing and polishing. In addition, samples for TEM were mounted on a fine copper support grid and thinned by conventional argon ion milling.

Scanning electron microscopy (SEM) was performed using a Cambridge S4-10 instrument. Transmission electron microscopy (TEM) employed a Philips EM400T machine operated at a voltage of 120 kV. Electron microprobe analysis was performed using a JEOL 733 Superprobe equipped with four wavelength dispersive spectrometers and a Tracor Northern 14500 energy dispersive system. All analyses were obtained using the WDS system. Operating conditions were 15 kV and 5 μA at a beam diameter of approximately 1 μm. Accuracy was ± 1.5–2.0% for the major elements.

X-ray fluorescence spectrometry was performed using a Philips PW1410 spectrometer. Samples were prepared using a modified form of the method of Norrish & Hutton (1969).

SLICKENSIDE CHARACTERISTICS

Mesoscopic features and sense indicators

Two structures resulted from excavator bucket–rock interaction: (1) scrape furrows, up to 0.5 m long, 8 cm wide (approximating a single tooth width) and <5 mm deep (Figs. 1a–c), which were locally covered by light-coloured, thin, shiny, brittle flakes of striated siliceous material (Fig. 1b), the majority of which lay unattached to the scrape furrow and were easily blown away by the wind (designated partly bonded to unbonded slickensides); and (2) darker, shiny, striated (grooved) coatings developed on the rock surface, typically 2 cm long and wide (designated fully bonded slickensides; Figs. 1d–f). Both the unbonded and bonded slickensides contain visible metallic fragments embedded in their surfaces. Most of the slickensides were found to be magnetic.

Significantly, the slickensides showed a number of features which could be related to the known sense of tooth movement. All striae were oriented parallel to the direction of excavator bucket–tooth movement (direction and sense indicated by the arrows in Figs. 1a–f). Certain of the scrape furrows comprise partly bonded slickensided 'flakes' that strike at right-angles to and dip in the same direction as the sense of tooth motion (circled in Figs. 1b & c). Steps of mainly accreted material are also developed, with their faces (risers) opposing the sense of tooth motion (Fig. 1b & c). Carrot-shaped grooves are commonly visible on the bonded slickensides. These also point in the opposite direction of tooth motion (i.e. they point in the same direction as the *relative* movement of the rock sample). A groove and associated ploughing element can be seen circled in Fig. 1(e). Crescent-shaped surface fractures and tears are also common, the tips of which point in the direction of tooth motion (circled in Fig. 1f).

SEM and TEM data: evidence for melting

Fragments of the excavator-generated bonded slickensides were examined in plan view using the SEM (Figs. 2a–f). Figure 2(a) reveals a general overview of the surface. It shows a number of grooves of different depths (the arrowed example 'g' is approximately 10 μm in width) set within a finely striated plateau which, in places, contain 'tear' structures (fractures) oriented at right-angles to the direction of shear (see arrow with 't'). These tears are shown enlarged in Fig. 2(b). They are usually <10 μm wide. Glassy 'highs' occur on the plateau (Fig. 2c).

At higher magnification, 'stringy' and 'sinewy' textures are revealed between the parted walls of the tears and within the bases of certain grooves (Figs. 2d–f). These are stretched out parallel to the direction of tooth motion. Figure 2(d) shows sinewy membrane material between mineral clasts in which oval holes and cavities are developed. Figure 2(e) shows similar material, but the connections between grains are more stretched and the groundmass has a more pervasively molten appearance. Some of the strings are rod-like and may drape over mineral clasts (Fig. 2f).

The difficulty of distinguishing between glasses and ultrafine particles using the conventional petrographic microscope and the SEM has led to some controversy in the literature (e.g. Wenk 1978, Maddock 1983). So,

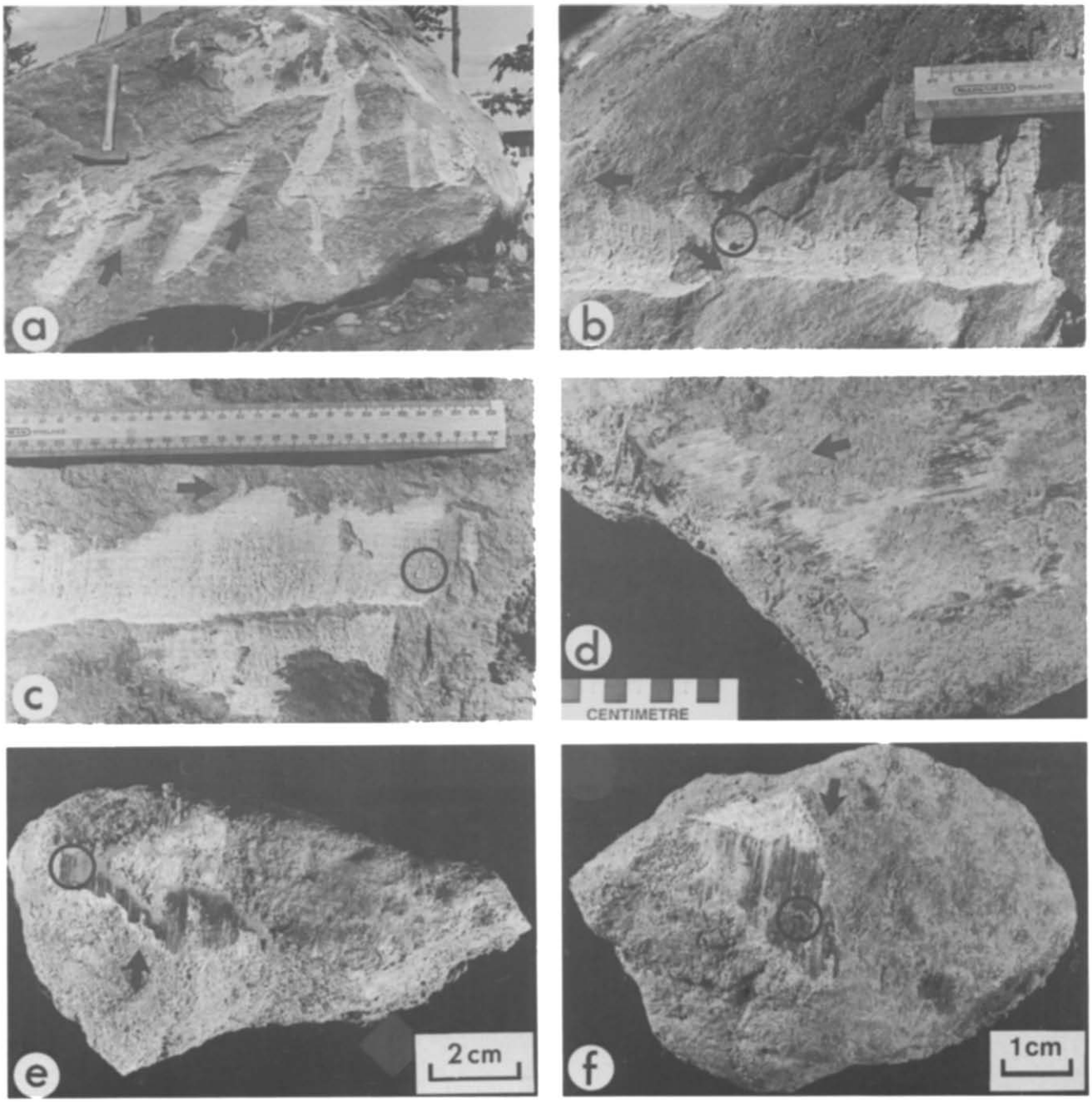

Fig. 1. Mesoscopic slickenside features. (a) Large sandstone boulder excavated by back shovel. Scrape furrows indicate where bucket teeth lost grip and slipped during lifting. Mainly unbonded slickensides were formed on these scraped surfaces, although accretion steps can also be observed. Arrows indicate the movement of the excavator tooth. (Hammer for scale.) (b) Back shovel scrape furrows generated in separate incidents by single tooth. Arrows indicate sense of tooth displacement. Partly attached, flaky slickensides were generated during left to right tooth movement (example circled). Accretion steps generated during earlier right to left tooth movement occur over the remaining area. (c) Partly attached slickensided 'flakes' (circled) that strike at right-angles to and dip in the direction of tooth motion. Steps of mainly accreted material are also developed (e.g. central and left portion of scrape furrow). As with (b), their faces oppose the sense of tooth motion. (d)–(f) Bonded, striated slickensides generated on boulders by front loader bucket. A groove and associated ploughing element are circled in (e). Tips of crescentic fractures in the slickensided surfaces, circled in (f), point in the direction of tooth motion.

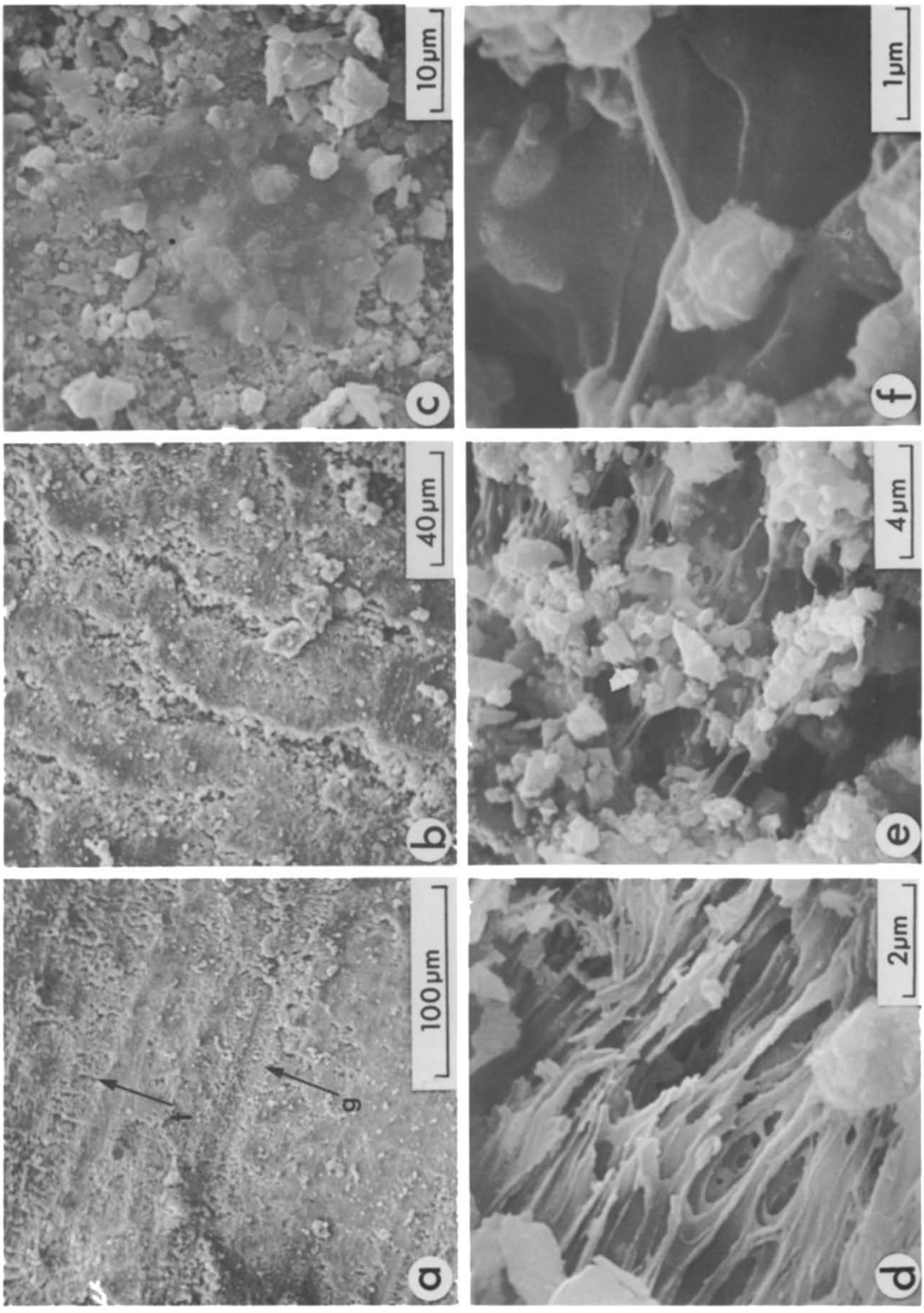

Fig. 2. SEM images of slickenside morphology. (a) Slickenside surfaces comprise grooves (see arrow with 'g') and intervening plateaux. Plateaux may be 'torn' (see arrow with 't'). (b) The plateaux are finely striated. Tears reveal some of the internal structure of the slickenside. (c) Other areas of the plateaux consist of 'glassy' highs. (d) (f) Higher magnification of the material within the tears reveals striae and molten textures.

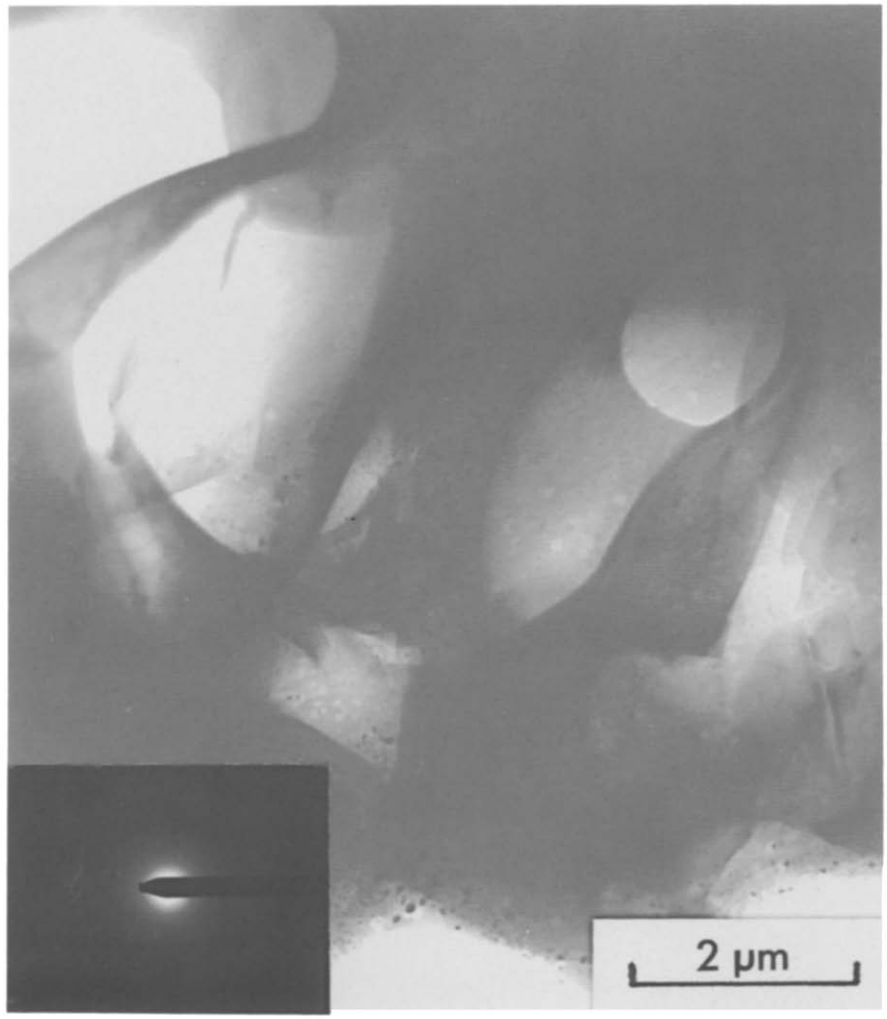

Fig. 3. Bright field TEM image of stringy material from sectioned slickenside (see Figs. 2d–f for SEM images of similar material). Electron diffraction pattern (inset) shows no evidence of crystallinity indicating that the material is amorphous (i.e. a glass). Minor Cu deposition, seen as small, dark circular precipitates at base of image, is due to Cu release from the fine support grid during argon ion milling.

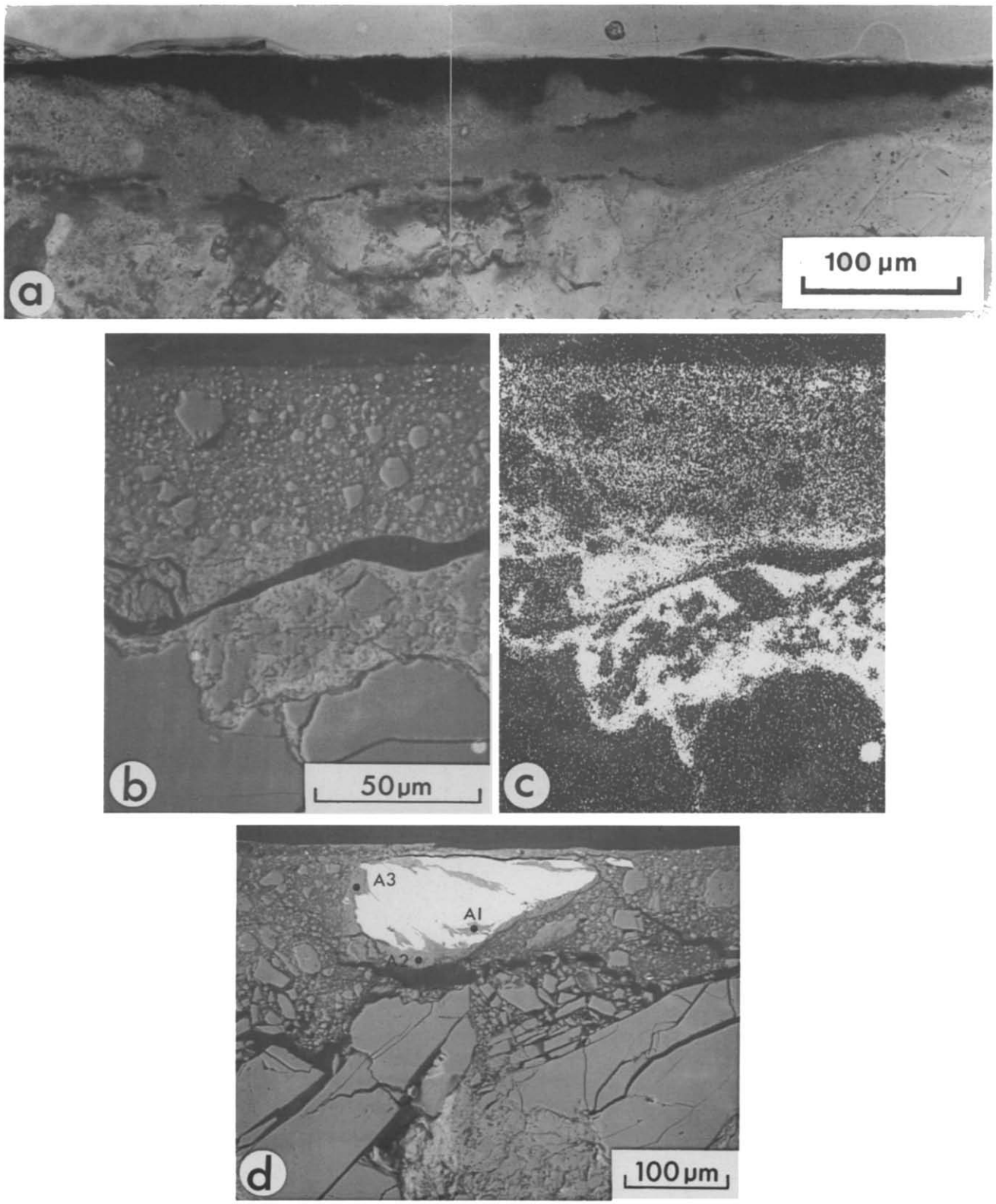

Fig. 4. Sectioned excavator-generated slickensides. (a) Transmitted light photomicrograph of section cut normal to slickenside surface. Note the opaque outer zone and its transition to the subjacent translucent zone. (b) Back scattered SEM/microprobe image of sectioned slickenside. Crack due to cooling. (c) Fe–Kα X-ray image of (b). (d) Back scattered SEM/microprobe image of a larger steel fragment, derived from front loader tooth, with silicate halo and injections. Data for microprobe points A1–3 are presented in Table 1. Note fractured condition of rock substrate.

while it appeared that a *melt* origin for the stringy material of the excavator-generated slickensides was plausible, it was decided to test this using the TEM.

Figure 3 is a TEM image of the stringy connecting material shown in Figs. 2(d)–(f). The electron diffraction pattern reveals that this material is amorphous (i.e. it is a glass). Care was taken not to confuse these strings with epoxy. However, the very same strings were observed using the SEM on samples that had not been epoxy impregnated (Figs. 2d–f). Furthermore, the epoxy was observed to occur only in massive form and not as strings.

In conclusion, the combined SEM and TEM data demonstrate that localized melting occurred during slickenside formation.

Internal structure and composition: evidence for bulk melting and Fe-enrichment

Using conventional light microscopy, two distinct surface-subparallel zones of varying thickness could be observed within the fully bonded slickensides: (1) an outer opaque zone, up to 50 μm thick; and (2) an underlying translucent zone, up to 50 μm thick (Fig. 4a). Using the microprobe, back scattered electron images of the sectioned surface reveal a clastic texture consisting of angular to sub-angular clasts set in an ultrafine matrix, with small steel fragments (bright spots) occurring within 10 μm of the surface (Fig. 4b). An Fe–Kα X-ray image of the same area shows that there is Fe-enrichment of the slickenside, especially of the lower layer (Fig. 4c).

Larger steel fragments were also incorporated into the slickenside, some of which are up to 100 μm in thickness (Fig. 4d). These usually lie with their longer axes oriented sub-parallel to the slickenside surface. Microprobe analyses of the steel fragments indicate a high-carbon steel composition for both sets of excavator teeth, approximating Fe (97%), Mn (2%) and C (1%). In many of the other sectioned slickensides, steel fragments were observed to occur throughout the entire thickness of the slickenside.

In addition to the outer opaque and translucent zones, back scattered imagery reveals a third structural layer to the slickensides: an innermost zone displaying varying degrees of fracture, up to 100 μm thick, where the original mineralogy and rock texture can be observed (Fig. 4d).

Large surface-subparallel fractures commonly separate the zones, especially the innermost fractured zone from the two outer zones (Figs. 4b & d). Where the zone-parallel fracturing was extensive, this may have resulted in 'unbonding' and facilitated loss of the slickenside from the surface. Unbonding and loss were found to be particularly common in slickensides generated by the back shovel.

Figure 4(d) also reveals the presence of a thin halo or 'aureole' around the steel fragment. The fragment shows evidence of having undergone ductile shear and associated gash formation whereupon halo material has become incorporated into the gashes (Fig. 4d).

Table 1 presents an XRF-determined whole rock composition of the sandstone and electron microprobe analyses of material located in and around the steel fragment shown in Fig. 4(d) (analytical points indicated by dots A1–3). The halo material is so fine grained that it could not be resolved on the SEM. The microprobe results do show some variation in composition, possibly reflecting the inclusion of submicroscopic mineral fragments but, within the limits of error, the mean composition for analyses A1–3 is comparable to the whole rock value. This implies that the sandstone was effectively homogenized in bulk to yield a submicroscopic mass, at least locally. Such homogenization would also be compatible with localized melting, as supported by the SEM and TEM data.

Varying amounts of Fe-enrichment also accompanied homogenization: the mean silicate halo contains 3.9% FeO vs 3.2% FeO for the whole rock, and analyses of the matrix show a more marked enrichment (M1 and M2, Table 1). These results are in keeping with the Fe-distribution map of Fig. 4(c).

INTERPRETATION

Figure 5 is a diagrammatic representation of slickenside formation during the mechanical excavation of rock. At any instant it is apparent that a number of deformation processes are occurring at the rock surface: (1) compression (directly in front of the tooth); (2) comminution and frictional heating (at the tooth–rock interface); and (3) cooling and extension (directly behind the tooth). It should be borne in mind that all three processes occur simultaneously and that it took considerably less than 1 s to form even the longest slickenside.

Table 1. Whole rock XRF analysis of sandstone protolith (column 1) with selected electron microprobe (WDS) data for slickensides. A1–3 are analyses of a silicate material adjoining a steel fragment (analysis points shown in Fig. 4d). Column 5 gives their mean. M1 and M2 are analyses of slickenside matrix (i.e. the material bonding the sandstone mineral fragments together). For comparative purposes, all analytical data have been normalized to 100% in a volatile-free state. The whole rock result included 2.7% H_2O, 0.2% CO_2, 1.61% FeO and 1.83% Fe_2O_3. Probe data comprise <4% volatiles. All iron reported in ferrous state (FeO*)

	Whole	Halo			Mean	Matrix	
Wt%	rock	A1	A2	A3	halo	M1	M2
SiO_2	80.0	76.5	78.3	85.9	80.2	81.1	77.5
TiO_2	0.6	0.6	0.0	0.1	0.2	0.1	0.2
Al_2O_3	11.1	13.5	12.8	6.6	11.0	8.5	9.6
FeO*	3.3	4.5	2.9	4.2	3.9	7.0	8.5
MnO	0.1	0.0	0.0	0.0	0.0	0.1	0.1
MgO	1.0	1.2	0.4	0.8	0.8	0.8	2.5
CaO	0.7	0.6	1.6	0.9	1.0	0.2	0.2
Na_2O	1.7	1.9	2.3	0.7	1.6	1.1	0.4
K_2O	1.5	1.2	1.7	0.8	1.2	1.1	1.0
Total	100.0	100.0	100.0	100.0	99.9	100.0	100.0

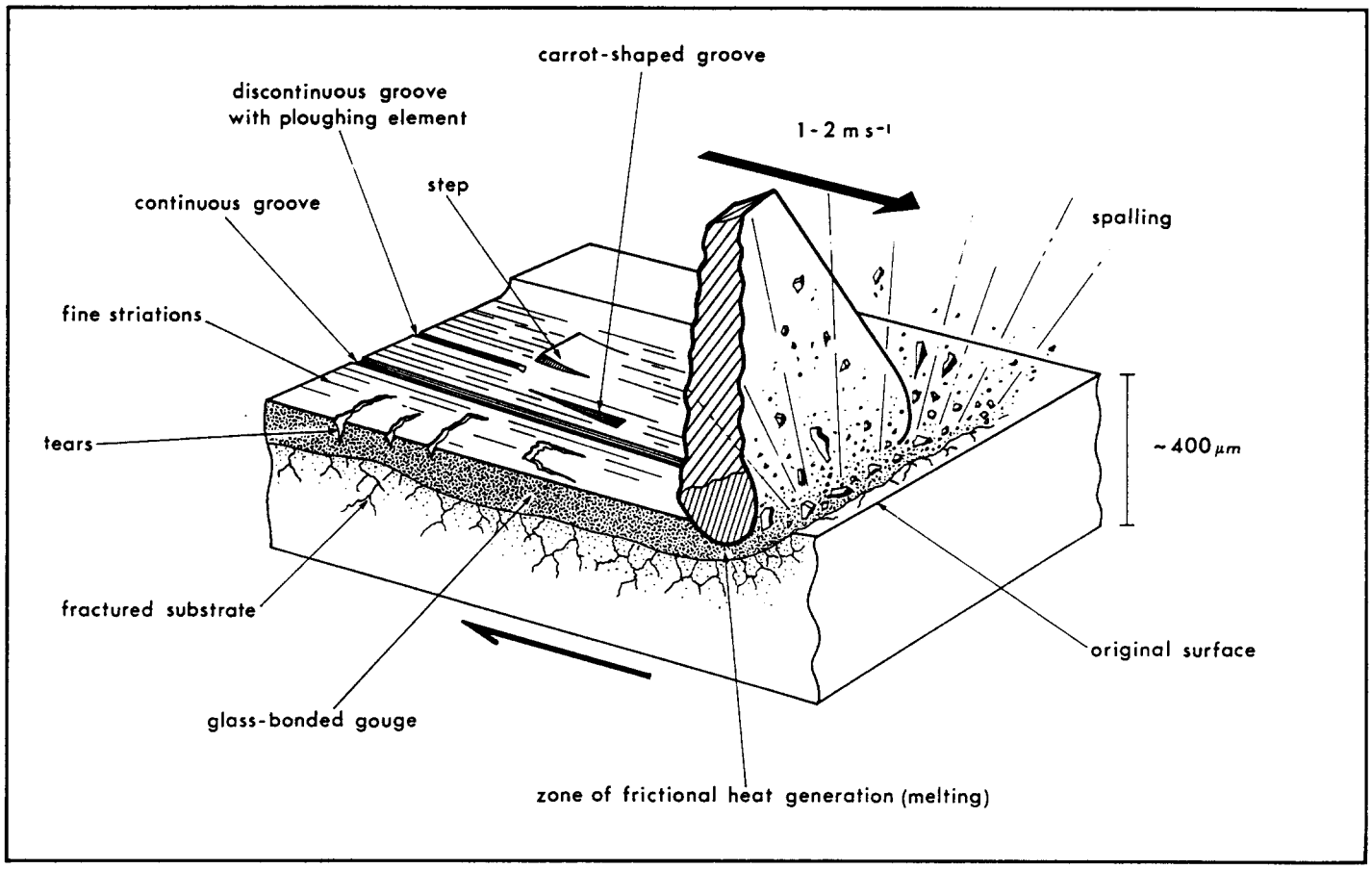

Fig. 5. Schematic representation of tooth–rock interaction leading to slickenside generation and formation of related surface features (see text for discussion). Tooth size reduced for clarity.

Compression

The explosive spalling of rock fragments and rock powder from the sandstone surface accompanied by a tearing sound was presumably due to brittle failure under unconfined conditions immediately ahead of the moving tooth, i.e. during the release of surface energy. This resulted in a net loss of material from the rock surface (Fig. 5). Loss of material was especially prevalent during back shovel excavation, whereby scrape furrows were developed (Figs. 1a–c). This could be attributed to the higher angle of tooth–rock interaction during shear, as opposed to the lower angle of tooth–rock incidence for the front loader.

Comminution and frictional heating

Directly beneath the tooth the rock was comminuted and, at the same time, confined under pressure resulting in no net loss of material. It is here that the frictional heat was generated as grain bonds were broken and individual grains fractured. The frictional heating resulted in the melting of the upper 100–150 μm of the rock surface.

It is clear that the tooth underwent wear during scraping because fragments of steel were transferred to the slickenside. The distribution of steel fragments throughout the thickness of the slickensides indicates that some form of mixing must have occurred. As an explanation, it is suggested that the silicate melt underwent turbulent flow immediately beneath the tooth so as to effectively disperse mineral clasts and steel fragments through the melt layer.

The origin of the Fe-enriched slickenside matrix can be attributed to the diffusion of iron from the steel tooth and its fragments into the surrounding silicate melt, possibly assisted by turbulent flow. Fe-enrichment does not necessarily require melting of the steel, but rather the chemical reaction of Fe with the silicate melt. Furthermore, it is known that the diffusion of Fe in a silicate melt is strongly temperature dependent and that Fe will tend to concentrate at the *lower* temperature end of a thermal gradient (e.g. Lesher & Walker 1986). This Soret-type effect explains the Fe gradient shown in Fig. 4(c), where the Fe concentration is observed to *increase* away from the slickenside surface (i.e. away from the source of heat).

As a result of the transfer of steel from the tooth to the slickenside, it is apparent that the wear of excavator teeth does not occur by physical abrasion alone but, in the case of the surface melting of silicates during rock excavation, also by the diffusion of Fe directly into frictionally-generated melt. Such thermally-activated wear of tools has been termed 'hot abrasion' (Perrott 1979). Hot abrasion effects could have been minimized in this instance if more appropriate tool materials had been used, i.e. alloy steel or tungsten carbide teeth.

Two interpretations are favoured for the formation of

the grooves on the slickensides. It is possible that the melt layer, once partly or completely frozen, could have been scraped by hard, refractory silicate particles (e.g. zircon) embedded in the trailing edge of the steel tooth. The observation that minute particles of silicate material are present at the tips of the excavators' teeth supports this interpretation. It is also possible that the tooth–rock interface was one of classic asperity contact (comprising steel and/or silicate asperities), whereby only parts of the tooth surface were in actual contact with the rock surface and vice versa. If so, then melt would be generated at the points of real contact and immediately flow to areas of lower pressure between asperities and pervade the inter-asperity gouge. In this case the grooves would represent the melt-generating asperity paths.

Cooling and extension

The melt would be supercooled in the wake of the tooth trajectory to leave a glassy veneer. For the partly bonded to unbonded slickensides, the presence of a transient but steep thermal gradient, followed by rapid cooling, would explain the cracking and potential exfoliation of the fused zone from the underlying fractured substrate and hence slickenside loss. The extensional regime developed behind the tooth could account for the development of surface tears (Fig. 2b) and inter-tear melt strings (Figs. 2d–f).

DISCUSSION

Comparisons with natural slickensides

The structures developed on the surfaces of the sandstone boulders during their excavation share many similarities with natural slickensides: they are planar, non-penetrative, shiny and grooved and show a number of damage features that can be related to the sense of slip.

Slip-parallel linear features on natural slickensides have been collectively referred to as slickenlines (Fleuty 1975) or slickenstriae (Weaver 1975) and currently include scratch, streak, tail, fibre, spike and nest structures (Means 1987). The striations of the artificial slickensides mainly comprise grooves (or scratches) of varying lengths, widths and depths.

The surface damage features of the artificial slickensides verify the commonly accepted *sense* indicators for natural slickensides: for example, the incongruous accretion steps of Norris & Barron (1969), the carrot-shaped grooves of Scholz & Engelder (1976) and the crescentic fractures or 'T' criteria of Petit (1987) and related 'lunules' of Wegmann & Schaer (1957), in which the tips of the crescents point in the direction of slip. Some controversy still exists with regard to reliably using the facing of steps as sense indicators (e.g. Paterson 1958, Gay 1970, Lindstrom 1974), but the artificial steps described in this work possess risers that face so as to oppose the sense of tooth displacement.

Heat production and temperature rise at the tooth–rock interface

Evidence for melting of the rock surface is supported by a consideration of heat production and temperature rise at the tooth–rock interface. Table 2 summarizes the slickenside generating conditions. Maximum loads are obtained from estimations of the weight of: (1) the largest boulder moved during back shovel excavation (6 m^3 at a mean density of 2500 kg m^{-3} for sandstone, which also approximates the machine's maximum lifting capacity); and (2) half the weight of the front loader, assuming that all the front axle weight is transferred to a single bucket tooth edge when a small rock boulder is encountered. The contact area (a) is for single tooth contact. Tooth velocities (V) approximated 1 m s^{-1} for the back shovel and 2 m s^{-1} for the front loader. For $\sigma_n < 200$ MPa the shear stress (τ) is obtained from $0.6\sigma_n$, and for $\sigma_n < 200$ MPa, $\tau = 0.85\sigma_n$ (Byerlee 1978). This yields a maximum heat production q at the tooth–rock interface of 175–200 MW m^{-2}. It is likely to have been considerably less than this where more than one tooth was in contact with rock or where smaller (lighter) boulders were manoeuvred by the back shovel. However, it was observed that slickensides tended to be formed preferentially under maximum shear stress conditions, i.e. when a high load was borne by a single tooth.

Establishing the *rate* of heat production for a moving source of heat yields an approximation of the temperature (T) at the surface of sliding contact, assuming that most of the energy is dissipated as heat (Engelder *et al.* 1975). The work of Jaeger (1942) is applicable here, wherein a solution for the mean temperature rise of the contact area between a sliding heat source (i.e. the excavator tooth) and a semi-infinite slab (i.e. the sandstone) is given by:

$$\Delta T = \frac{4qf}{3k\sqrt{\pi}}\left(\frac{kL}{\varrho cV}\right)^{1/2}.$$

For the bonded slickensides produced by the front loader: $q = 2 \times 10^8$ W m^{-2}; f (fraction of frictional heat flowing into rock) = 0.5; k (thermal conductivity) = 3 Wm^{-1} °C^{-1}; ϱ (density) = 2500 kg m^{-3}; c (specific heat) = 1000 J kg^{-1} °C^{-1}; V (velocity) = 2 m s^{-1}; and L (tooth length in direction of movement) = 5×10^{-3} m and the resulting ΔT is 1400°C. For the partly bonded to

Table 2. Parameters for tooth–rock heat production (q) determination. σ_n in MPa is obtained from $0.2Y \times 0.09807$, given Y = 15,000 kg for the back shovel and Y = 6000 kg for the front loader, where Y is distributed over an estimated tooth–rock contact area (a) of 5 cm^2. $\mu \approx 0.6$ for $\sigma_n > 200$ MPa (back shovel) and ≈ 0.85 for $\sigma_n < 200$ MPa (front loader)

Excavator	σ_n (MPa)	μ	a (m^2)	V (m s^{-1})	$\tau = \mu\sigma_n$ (MPa)	$q = \tau V$ (MW m^{-2})
Back shovel	≤294	0.6	5×10^{-4}	1	176	176
Front loader	≤117	0.85	5×10^{-4}	2	100	200

unbonded slickensides produced by the back shovel: $q = 1.76 \times 10^8$ and $V = 1$ ms^{-1} (all other parameters being the same as for the front loader), and the resulting ΔT is 1700°C.

These results assume that the heat is partitioned equally between the tooth and rock (see Berry & Barber 1984, for a more elaborate account of this problem) and that the cooling effects of turbulence within the melt layer and heat radiation from the surface are neglected. Nevertheless, the temperatures obtained are reasonable and indicate that virtually all the mineral phases present in the sandstone would have been melted by frictional heating (e.g. the back shovel-generated slickensides attained a temperature close to the melting point of monomineralic quartz rock). This is in good agreement with the analytical evidence for bulk melting.

In general, flash temperatures (e.g. at asperity contacts) would have exceeded the *mean* surface temperatures as obtained from Jaeger's formula, but the maximum temperatures realized would have been buffered by the melting points of the constituent mineral phases (e.g. Bowden & Tabor 1950), most of which were quartz and feldspar.

Slickensides as indicators of palaeoseismicity

The shear stresses and slip rates leading to the formation of the excavator-generated slickensides are comparable to high stress and transitory high strain rate conditions of seismic faulting. Estimates of average tectonic shear stress within crustal fault zones range between 10 and 100 MPa (Hanks & Raleigh 1980), while seismic slip rates of 0.1–2 m s^{-1} are likely to occur for a few seconds in a stick–slip regime (Brune 1976, Sibson 1980). This yields a maximum heat production of 200 MW m^{-2} and one that is comparable to the energy released during excavator-generated slickenside formation (Table 2). The recognition of natural slickensides which are demonstrably produced by frictional melting would indicate that relatively large seismic events have occurred on the generating surface in the geological past.

In the case of the excavator-generated slickensides it is reasonable to equate the intermittent tearing sound released from the tooth–rock interface to stick–slip behaviour. Engelder (1974) and Scholz & Engelder (1976) have suggested that the development of carrot-shaped grooves can be related to the ploughing of asperities during slip and their subsequent seizure to locking (stick). The generation of similar features as well as steps on the artificial slickensides may have been the cause of jerky tooth–rock interaction and hence discontinuous acoustic emission.

CONCLUSIONS

The excavator-generated slickensides described in this work were formed under transient and relatively high stress–high velocity conditions comparable to co-seismic faulting. The energy released at the tooth–rock interface resulted in the comminution and frictional melting of the sandstone surface and the assimilation of Fe from the excavator teeth into a silicate liquid. A section through one of these slickensides reveals a ≤150 μm thick structure comprising glass-bonded gouge containing minor steel fragments. An underlying substrate, ≤100 μm thick, consists of fractured but otherwise unaltered sandstone. The total thickness of the modified surface layer is therefore ≤250 μm.

The excavator-generated slickensides are similar to natural slickensides and verify some of the commonly used sense indicators of their natural counterparts. In contrast, evidence of melting appears to be lacking in natural slickensides, even though this work indicates that melting should be commonplace.

Obviously, caution should be exercised when making comparisons between artificial slickensides generated on a free surface by a single steel indenter and natural slickensides formed under a confining pressure on a fault surface. However, the excavator tooth could be considered a single large asperity and the resulting scrape furrows as large grooves. In this respect asperities may show self-similarity and so occur at a number of scales ranging, in this case, from the size of a steel indenter down to molecular or atomic dimensions.

A critical difference between the experiments described here and faulting may lie in the negligible effects of pore-fluid pressure occurring at the tooth–rock interface. For 'wet' faulting, frictional heating will tend to expand pore fluid and induce a pressure increase that could relieve the shear stress and inhibit surface melting. This may account for the apparent restriction of friction melts to conditions of relatively 'dry' faulting as shown by field and laboratory studies (e.g. Spray 1987, 1988).

This work also suggests that compositional–textural end-members exist: primary slickensides generated directly from the wall rock material (e.g. gouge or fused gouge) and secondary slickensides consisting of recrystallized primary slickensides or precipitations from extraneous fluids (e.g. slickenfibres). In an actively evolving slip system both types are likely to be present. The primary and secondary forms may correlate with seismic and interseismic displacement, respectively (cf. Wise *et al.* 1984). The slickensides described in this work are clearly primary, whilst most exhumed natural slickensides are likely to be more evolved and show secondary features.

Preservation of a co-seismic friction-melt phase of slickenside development is likely to be less common than the survival of slickensides formed by gouge induration and mineral coating. This is because lengthier periods of interseismic behaviour would favour devitrification and the development of a modified surface that would tend to obscure or destroy earlier evidence for the existence of a glass veneer. In this respect it would be best to look for indications of surface melting in slickensides generated on a recently active and freshly exposed fault surface.

Acknowledgements—This work was funded by grant A1455 awarded to the author by the Natural Sciences and Engineering Research

Council of Canada. I thank Joseph Clancy White for discussions and for advice on TEM analysis, and Win Means and Paul Williams for commenting on an earlier version of the manuscript. SEM and TEM analyses were performed with the assistance of David Rae and Susan Belfry at the Electron Microscopy Unit of the University of New Brunswick (operated with the support of an NSERC infrastructure grant). Microprobe analysis was performed at Dalhousie University, Nova Scotia.

REFERENCES

Barss, M. S. & Hacquebard, P. A. 1967. Age and stratigraphy of the Pictou Group in the Maritime Provinces as revealed by fossil spores. *Spec. Pap. geol. Ass. Can.* **4**, 267–283.

Berry, G. A. & Barber, J. R. 1984. The division of frictional heat—a guide to the nature of sliding contact. *J. Tribol.* **106**, 405–415.

Bowden, F. P. & Tabor, D. 1950. *The Friction and Lubrication of Solids*. Clarendon Press, Oxford.

Brace, W. F. & Byerlee, J. D. 1966. Stick–slip as a mechanism for earthquakes. *Science* **153**, 990–992.

Brune, J. 1976. The physics of earthquake strong motion. In: *Seismic Risk and Engineering Decision* (edited by Lomnitz, C. & Rosenblueth, E.). Elsevier, Amsterdam, 141–147.

Byerlee, J. D. 1978. Friction of rocks. *Pure & Appl. Geophys.* **116**, 615–626.

Durney, D. W. & Ramsay, J. G. 1973. Incremental strains measured by syntectonic crystal growths. In: *Gravity and Tectonics* (edited by DeJong, K. A. & Scholten, R.). John Wiley and Sons, New York, 67–96.

Engelder, J. T. 1974. Microscopic wear-grooves on slickensides: indicators of paleoseismicity. *J. geophys. Res.* **79**, 4387–4392.

Engelder, J. T., Logan, J. M. & Handin, J. 1975. The sliding characteristics of sandstone on quartz fault-gouge. *Pure & Appl. Geophys.* **113**, 68–86.

Fleuty, M. J. 1975. Slickensides and slickenlines. *Geol. Mag.* **112**, 319–321.

Friedman, M., Logan, J. M. & Rigert, J. A. 1974. Glass-indurated quartz gouge in sliding-friction experiments on sandstone. *Bull. geol. Soc. Am.* **85**, 937–942.

Gay, N. C. 1970. The formation of step structures on slickensided shear surfaces. *J. Geol.* **78**, 523–532.

Hanks, T. C. & Raleigh, C. B. 1980. The conference on magnitude of deviatoric stresses in the Earth's crust and upper mantle. *J. geophys. Res.* **85**, 6083–6085.

Hills, E. S. 1972. *Elements of Structural Geology* (2nd edn). Chapman & Hall, London.

Hobbs, B. E., Means, W. D. & Williams, P. F. 1976. *An Outline of Structural Geology*. Wiley & Sons, New York.

Jaeger, J. C. 1942. Moving sources of heat and the temperature at sliding contacts. *J. Proc. New South Wales* **76**, 203–224.

Jaeger, J. C. 1959. The frictional properties of joints in rock. *Pure & Appl. Geophys.* **43**, 148–158.

Lesher, C. E. & Walker, D. 1986. Solution properties of silicate liquids from thermal diffusion experiments. *Geochim. cosmochim. Acta* **50**, 1397–1411.

Lindstrom, M. 1974. Steps facing against the slip direction. *Geol. Mag.* **111**, 71–74.

Maddock, R. H. 1983. Melt origin of fault-generated pseudotachylytes demonstrated by textures. *Geology* **11**, 105–108.

Means, W. D. 1987. A newly recognized type of slickenside striation. *J. Struct. Geol.* **9**, 585–590.

Norris, D. K. & Barron, K. 1969. Structural analysis of features on natural and artificial faults. In: *Research in Tectonics* (edited by Baer, A. J. & Norris, D. K.). *Geol. Surv. Pap. Can.* **68-52**, 136–167.

Norrish, K. & Hutton, J. J. 1969. An accurate X-ray spectrographic technique for the analysis of a wide range of geological samples. *Geochim. cosmochim. Acta* **33**, 431–453.

Paterson, M. S. 1958. Experimental deformation and faulting in Wombeyan marble. *Bull. geol. Soc. Am.* **69**, 465–476.

Perrott, C. M. 1979. Tool materials for drilling and mining. *Annu. Rev. Mater. Sci.* **9**, 23–50

Petit, J. P. 1987. Criteria for the sense of movement on fault surfaces in brittle rocks. *J. Struct. Geol.* **9**, 597–608.

Power, W. L. & Tullis, T. E. 1989. The relationship between slickenside surfaces in fine-grained quartz and the seismic cycle. *J. Struct. Geol.* **11**, 879–893.

Scholz, C. H. & Engelder, J. T. 1976. The role of asperity indentation and ploughing in rock friction—I. Asperity creep and stick-slip. *Int. J. Rock Mech. & Mining Sci.* **13**, 149–154.

Sibson, R. H. 1980. Power dissipation and stress levels on faults in the upper crust. *J. geophys. Res.* **85**, 6239–6247.

Spray, J. G. 1987. Artificial generation of pseudotachylyte using friction welding apparatus: simulation of melting on a fault plane. *J. Struct. Geol.* **9**, 49–60.

Spray, J. G. 1988. Generation and crystallization of an amphibolite shear melt: an investigation using radial friction welding apparatus. *Contr. Miner. Petrol.* **99**, 464–475.

Tjia, H. D. 1964. Slickensides and fault movements. *Bull. geol. Soc. Am.* **75**, 638–686.

Tjia, H. D. 1967. Sense of fault displacements. *Geol. Mijnb.* **46**, 392–396.

Weaver, J. D. 1975. A reply to: Slickensides and slickenlines, by M. J. Fleuty. *Geol. Mag.* **112**, 321–322.

Wegmann, E. & Schaer, J-P. 1957. Lunules tectoniques et traces de mouvements dans les plis du Jura. *Eclog. geol. Helv.* **50**, 491–496.

Wenk, H. R. 1978. Are pseudotachylites products of fracture or fusion? *Geology* **6**, 507–511.

Williams, G. D. & Spray, J. G. 1979. Non-cylindrical, flexural slip folding in the Ardwell Flags—a statistical approach. *Tectonophysics* **58**, 269–277.

Wise, D. U., Dunn, D. E., Engelder, J. T., Geiser, P. A., Hatcher, R. D., Kish, S. A., Odom, A. L. & Schamel, S. 1984. Fault-related rocks: suggestions for terminology. *Geology* **12**, 391–394.